Noninvasive Determination of Absorption and Reduced Scattering Coefficients of Adult Heads by Time-Resolved Reflectance Measurements for Functional Near Infra-Red Spectroscopy

T. Tanifuji-*EMBS Member*, and L. Wang, *Non-Member*

***Abstract*— Absorption and reduced scattering coefficients (μ_a and μ_s') of adult heads have been noninvasively determined by time-resolved reflectance measurements. The finite difference time domain (FDTD) analysis was used to calculate time-resolved reflectance from realistic adult head models with brain grooves containing a non-scattering layer. *In vivo* time-resolved reflectances of human heads were measured by a system composed of a time-correlated single photon counter and a diode laser. By minimizing the objective functions that compare theoretical and experimental time resolved reflectances, μ_a and μ_s' of brain were determined. It became clear that time-resolved measurements have enough sensitivity to determine both μ_a and μ_s' for superficial tissues, gray matter and white matter, except μ_s' for white matter.**

I. Introduction

Functional near infrared spectroscopy (NIRS) is widely used to non-invasively measure oxygenation in human brain and other tissues [1]. Multi-channel continuous-wave (CW) functional NIRS systems have been developed and are most commonly used to measure brain activity in clinical applications [1]. However, CW techniques suffer from poor depth sensitivity. In principle, time-resolved techniques can achieve greater penetration depths for measurements of the head with long delay times [2]. Therefore, great efforts have been made to develop a time-resolved system by employing diffuse optical tomography [3,4]. Time-resolved diffuse optical tomography (TR-DOT) involves minimizing an objective function that compares the predicted and measured time-resolved reflectances emitted from a body [3].

In this paper, TR-DOT for determining noninvasively the optical parameters (i.e., the absorption and reduced scattering coefficients, μ_a and μ'_s, respectively) of adult heads is estimated. The finite difference time domain (FDTD) analysis [5] was used to calculate time-resolved reflectance from realistic adult head models with brain groves containing a nonscattering layer [6] and with the curved surfaces [7]. *In vivo* time-resolved reflectances of human heads are measured by a system composed of a time-correlated single photon counter and a diode laser [8]. Objective functions are defined that compare the theoretical and experimental time-resolved reflectances. The optical parameters defined in the brain model are determined by minimizing the objective functions utilizing the conjugated gradient optimization [3]. It became clear that the optimization process successfully predicts μ_a and μ_s', and the mean delay (MD) and time-resolved reflectance calculated using the FDTD analysis are in agreement with *in vivo* experiments.

Resrach supported by a Grant-in-Aid for Scientific Research (No. 21560425) from the Ministry of Education, Culture, Sports and Technology, Japan

The Authors are with the Kitami Institute of Technology, Kitami-City, Hokkaido, 090-8507, Japan (corresponding author to provide phone/fax: +81-157-26-9296; e-mail: tanifuji@mail.kitami-it.ac.jp).

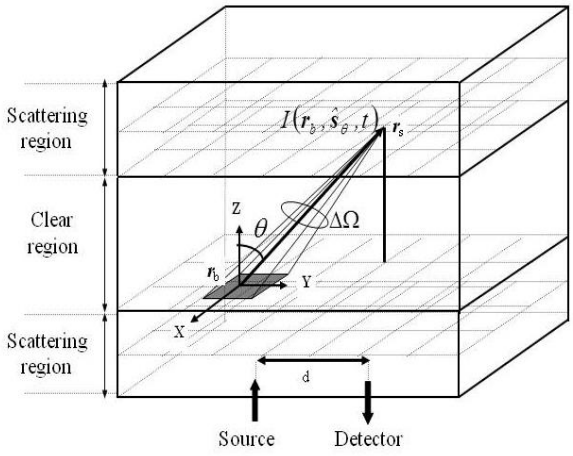

Figure 1. Optical coupling between scattering regions through a non-scattering region. $\mathbf{r}_s$ and $\mathbf{r}_b$ are located at the interface between the scattering and non-scattering region.

II. Theory for Predicting Time-Resolved Reflectance from Adult Heads

A. FDTD analysis of time-resolved reflectance from an adult head model

Fig. 1 shows a schematic of the FDTD analysis of a scattering medium containing a nonscattering (clear) region [6]. The dotted lines indicate the Yee grid used for FDTD analysis [5]. FDTD analysis is used to compute fluence rate $\phi(\mathbf{r},t)$ and all the components of radiant flux $\mathbf{J}(\mathbf{r},t)$ in each Yee grid cell in the scattering regions, which are illuminated by an isotropic point source. The radiance of the light emerging from the opposite side of the lower scattering layer $\mathbf{I}(\mathbf{r}_b, \hat{\mathbf{s}}, t)$ is given by [9]

$$I(\mathbf{r}_b, \hat{\mathbf{s}}, t) = \frac{\phi(\mathbf{r}_b, t)}{4\pi} + \frac{3}{4\pi}\left[J_n(\mathbf{r}_b, t)\hat{\mathbf{n}} + J_t(\mathbf{r}_b, t)\hat{\mathbf{t}}\right]\cdot \hat{\mathbf{s}}, \quad (1)$$

where $\boldsymbol{J}(\mathbf{r},t)$ was separated into outward normal and tangential components, $J_n(\mathbf{r},t)$ and $J_t(\mathbf{r},t)$,with respect to the non-scattering layer boundary. $\hat{\mathbf{n}}$ and $\hat{\mathbf{t}}$ are unit vectors

normal and tangential to the boundary, respectively. The space invariance of the specific intensity along a ray in free space [9] was used to calculate the specific intensity incident on the upper scattering medium on the opposite side of the clear layer, $\mathbf{I}_i(\mathbf{r}_s,\hat{\mathbf{s}},t)$, which is given by $\mathbf{I}_i(\mathbf{r}_s,\hat{\mathbf{s}},t)=\mathbf{I}(\mathbf{r}_b,\hat{\mathbf{s}},t)e^{-\mu_a|\mathbf{r}_b-\mathbf{r}_s|}$. Snell's law is then used to calculate the transmitted and reflected specific intensities in the upper and lower scattering media with an index mismatch at the boundary. As a result, the incident power $P_t(\boldsymbol{r}_s,t)$ of the diffuse light from the lower scattering medium propagating to the upper scattering medium is calculated [5]. The additional source $\varepsilon(\mathbf{r},\hat{\mathbf{s}},t)$ at $\boldsymbol{r}_s$ is then evaluated [5]:

$$\varepsilon(\mathbf{r}_s,\hat{\mathbf{s}}_{\theta_2},t)=\frac{1}{4\pi}\frac{\mu_s' P_t(\mathbf{r}_s,t)}{\mu_a+\mu_s'}\delta(\mathbf{r}-\mathbf{r}_s). \quad (2)$$

The additional source on the surface of the scattering layer is introduced into the diffusion equations by employing the new boundary conditions [5]. The additional source on the lower scattering layer due to the radiance from the upper scattering layer and the internal reflection at the boundary are accounted for in a similar manner.

B. *The influences of brain groove and the surface curvature on mean delay and time-resolved reflectance*

Fig. 2 shows a realistic adult head model [6] which has the fold like features known as gyri and the grooves in between known as sulci. Fig. 3(a) shows the MD dependences on *d* for three types of adult head. A Gaussian input pulse with a 1/*e* full width of 60 ps was used; the previously reported values of μ_a and μ_s' [6] in each layer were used in the calculation. By removing the CSF layer and brain groove from the model, MD increases linearly with respect to source-detector separation (*d*) as shown in Fig. 3(a). MD increases slowly with *d* for *d* larger than 30 mm in the presence of CSF as shown by the solid lines in the figure. Comparing the MD of the models with and without groove, the sulci filled with non-scattering CSF decreases MD because light transport is almost rectilinear in CSF. On the other hand, there is almost no change in MD and the time-resolved reflectance even if the source/detector positions are moved on the surface in the model. This is due to flattening of the intensity near gray matter and sulci due to the light scattering in the outer layer [7].

The dotted lines in Fig. 3(a) show MD dependences on *d* considering curvature of the head surface. As a measure of the curvature, the visibility length l_v = 30 mm is assumed [7]. Curvature considerably increases MD because optical piping effects due to $\varepsilon(\mathbf{r},\hat{\mathbf{s}},t)$ given by (2) are relaxed. Figure 3(b) shows the time-resolved reflectance for the model without CSF and the model with groove shown in Fig.2 assuming l_v = 30 mm. As predicted from Fig. 3(a), the peak delay differences of the time-resolved reflectances in both cases become remarkable as *d* exceeds 30 mm. The pulse profile itself is a critical factor in determining μ_a and μ_s'. The rising and falling slopes near the peaks are also influenced by CSF and these influences have large weight in the least square minimization discussed in later sections. Considering the above results, it is essential to use a realistic head model

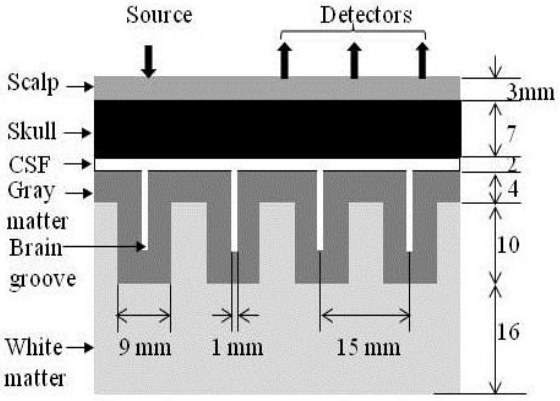

Figure 2. Schematic illustrations of the adult head model

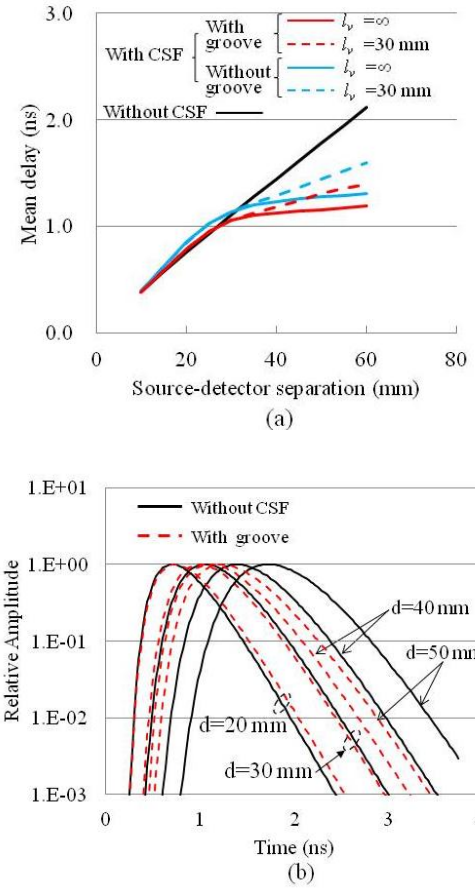

Figure 3. (a) MD dependence on d for three types of head model, and (b) time-resolved reflectance for two head models

because TR-DOT is usually operated with a multi source-detector apparatus [3, 4].

III. *IN VIVO* MEASUREMENT OF TIME-RESOLVED REFLECTANCE FROM ADULT HEADS

A. *Measurement system*

The output pulse of the semiconductor laser diode, operating at 680 nm, was launched into a plastic optical fiber 1 mm in core diameter to illuminate the volunteer's heads. The

reemitted diffuse light was collected by a 2 mm fiber bundle composed of thin clad multimode fibers 50 μm in diameter with a numerical aperture of 0.5. The illumination power was limited to less than 10 mW for safety reasons. For detection, we used a micro channel plate photomultiplier tube (R3809U-50, Hamamatsu Photonics K.K., Japan) and a time-correlated single-photon counter (SPC-330, Becker and Hickl GmbH, Germany). Figure 4 shows the instrument response function measured by feeding a small fraction of the plastic fiber output into the photomultiplier tube. The FWHM was 60 ps and was used as the input pulse for the FDTD analysis

B. *Protocol for* in vivo *measurements*

Three healthy male volunteers (21, 22, and 64 years old) were enrolled for measurements after informed consent. Measurements were performed by putting the injection and collection fibers on the left semi-sphere of the head at d = 20, 30, 40 mm, with the injection fiber placed toward the temporal region [8]. The surface profiles was measured for only one volunteer. The relations between l_v and MD agree with FDTD analysis shown in Fig.3(a).

IV. NON-INVASIVE DETERMINATION OF THE OPTICAL PARAMETERS OF BRAINS

The μ_a and μ_s' values of brains are estimated by minimizing the objective function that compares the theoretical and measured time-resolved reflectances. In this study, optical parameter determination was focused on one volunteer whose data were analyzed in more detail in the previous section. The μ_a and μ_s' of individual Yee cells are determined using TR-DOT. However, in this study, the problem is simplified and averaged values of μ_a and μ_s' within each layer are determined. It was assumed that CSF is nonscattering, *i.e.* μ_s'=0, and μ_a = 0.004 mm^{-1} [6] and was therefore not considered in the optimization process. In this case, the number of unknown optical parameters is eight.

A. *The objective function and its minimization process*

The objective function is defined as

$$\chi^2(\varsigma) = \sum_{s\in M}\sum_{n} \frac{\left[Y_s^n - J_s^n(\varsigma)\right]^2}{2\sigma(s,n)^2}, \qquad (3)$$

where the values of Y_s^n denote the measurement of the diffuse intensity $J_s^n(\varsigma)$ calculated for the optical properties ς =[μa, μ_s'], using the realistic head model shown in Fig. 2. The first sum over s indicates a summation over source-detector pairs, and the second sum over n represents the summation over the fitting range of the time steps, including all time steps with a number of counts higher than 10 % of the peak value on the rising edge of the reflectance and 1 % on the falling edge. The parameter $\sigma(s,n)$ is the noise variance, which is related to Y_s^n by $\sigma(s,n)^2 = Y_s^n . J_s^n(\varsigma)$ was calculated assuming l_v = 30 (mm) in the model. The minimization process was performed iteratively using the conjugated gradient (CG) method. The gradient vector of the objective function with respect to ς was calculated numerically and the conjugated vector was calculated from the result. Then, the minimum of the objective function was determined from the conjugated vector. Successive line minimization processes are used to obtain the global minimum of the objective function [3].

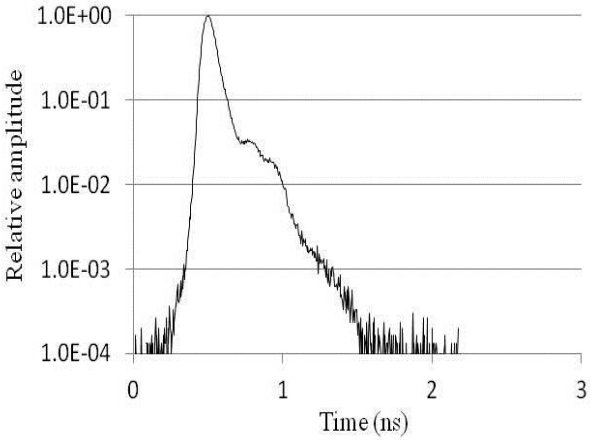

Figure 4. Instrument response function

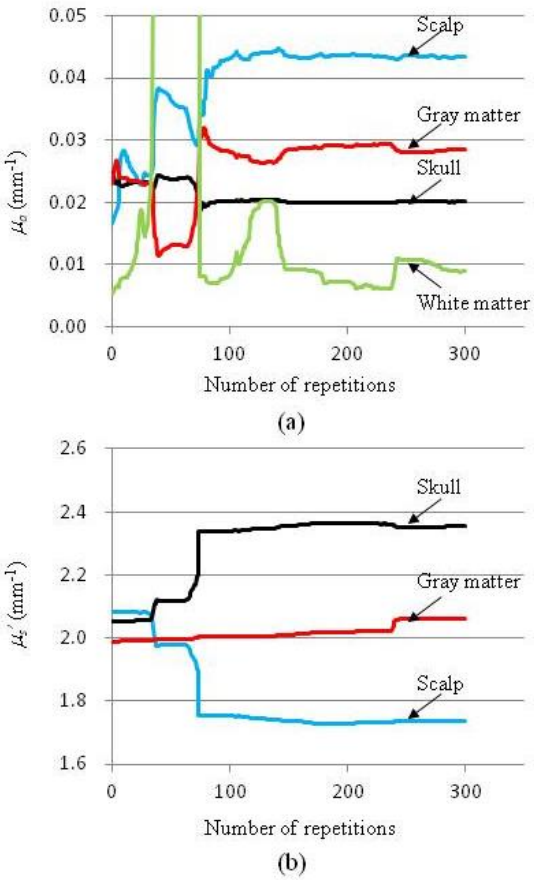

Figure 5. Optical parameter determination using the conjugated gradient optimization using the reflectance at d= 20, 30 and 40 mm. (a) μ_a for scalp, skull, gray and white matter, (b) μ_s' for scalp, skull, and gray matter.

B. *Optical parameter determination*

The reflectances at d = 20, 30 and 40 mm were used. The same initial values for μ_a and μ_s' were assumed as in the previous optimization process at 780 nm [7]. Figs. 5(a) and (b) show

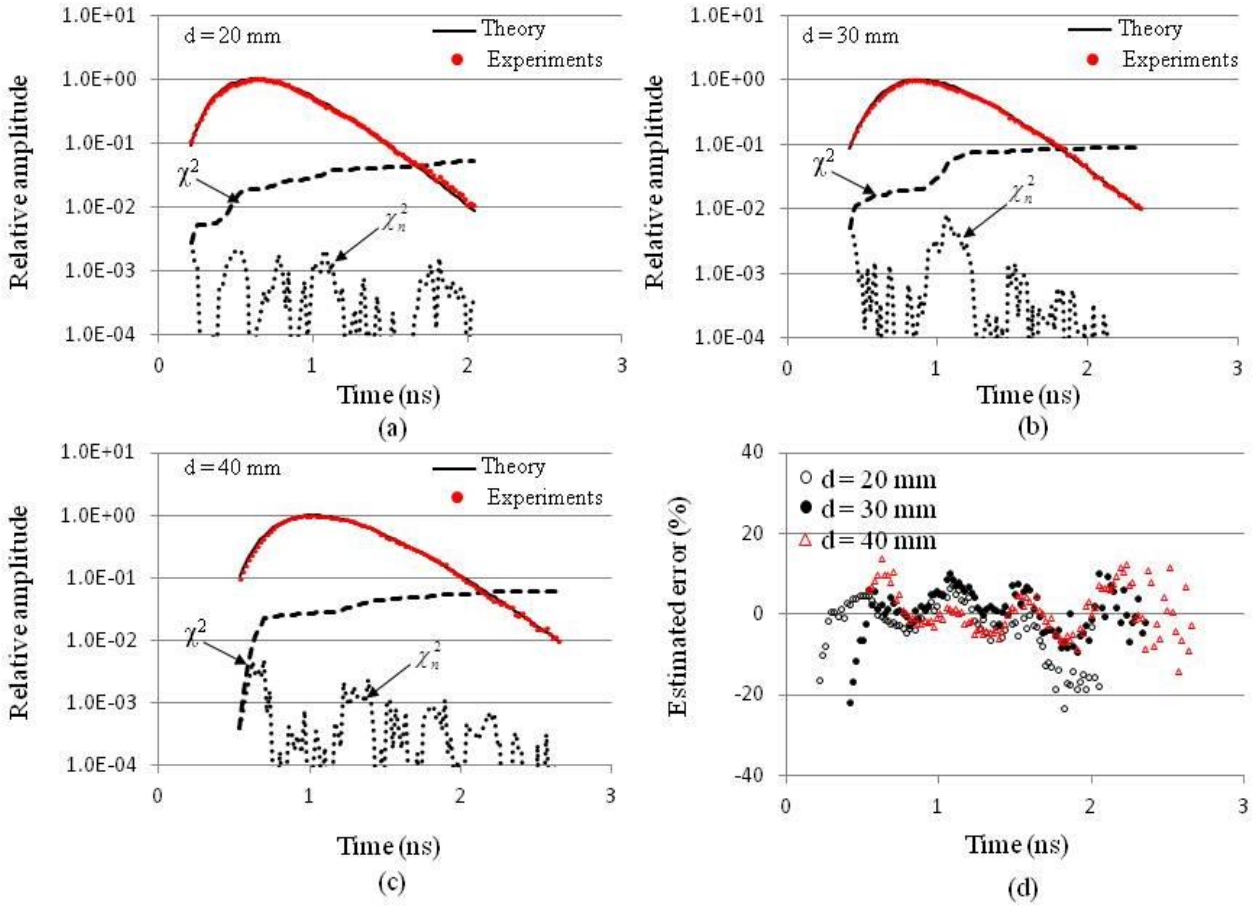

Figure 6. Theoretical and experimental reflectance for (a) d = 20 mm, (b) d = 30 mm, (c) d = 40 mm. (d) Error in theoretical reflectance amplitude.

the values of μ_a and μ_s' improved by using CG optimization, respectively. It became clear that the value of μ_a in all scattering layers converged to a global minimum. However, μ_s' in white matter changed by less than 10^{-2} % from the initial value. The other values of μ_s' converged to a global minimum. Figs. 6(a), (b) and (c) show the theoretical and experimental reflectances for d = 20, 30 and 40 mm, respectively, together with the temporal and cumulative square errors, χ_n^2 and χ^2 given by (3); the estimated amplitude errors are shown in Fig. 6(d). The theoretical reflectance agrees reasonably well with the experiments, which suggests time-resolved measurements have enough sensitivity to determine μ_a for white matter. It is necessary to improve the sensitivity over the rising and falling edges of the pulse to determine μ_s' of deep layers such as white matter. The optical parameters determined in this study are in good agreement with the previously reported values [6].

V. Conclusion

Our results indicate that time-resolved techniques can potentially be applied to visualize brain activity; however, significant improvements in both the theory and measurement systems are necessary to realize *tomographic* brain activity visualization based on time-resolved techniques.

References

[1] M. Fabiani, D. D. Schmorrow, and G. Gratton, et al., "Optical imaging of the intact human brain (guest editorial)," IEEE Eng. Med. Biol. Mag. vol. 26, pp.14-58, July/August 2007.

[2] R. D. Frostig, , *In vivo optical imaging of brain function*. Boca Raton FL: CRC Press, ch. 8, 2002.

[3] A. H. Hielscher, A. D. Klose, and K. M. Hanson, "Gradient based iterative image reconstruction schema for time-resolved optical tomography," IEEE Trans. Med. Imag., vol. 18, pp.261-271, March 1999.

[4] D. Contini, A. Torricelli, A. Pifferi, L. Spinelli, F. Paglia, and R. Cubeddu, "Multi-channel time-resolved system for functional near infrared spectroscopy," Opt. Exp., vol. 14, pp. 5418-5432, June 2006.

[5] T. Tanifuji, N. Nishio, K. Okimatsu, T. Tabata, , and Y. Hashimoto, "Finite difference time domain analysis of time-resolved reflectance from an adult head model composed of multilayered structure," Appl. Opt. vol. 51, pp. 429-438, Feb. 2012.

[6] E. Okada, and D. Delpy, "Near-infrared light propagation in an adult head model. I. Modeling of low-level scattering in the cerebrospinal fluid layer, " Appl. Opt. vol. 42, pp. 2906-2914, June 2003.

[7] T. Tanifuji, and M. Suzuki, "Theory and experiments on time-resolved reflectance from adult heads for functional tomographic imaging of brain activities", Proc. SPIE 8941, Feb. 1-6 2014.

[8] D. Comelli, A. Bassi, A. Pifferi, A. Torricelli, R. Cubeddu, F. Martelli, and G. Zaccanti, "In vivo time-resolved reflectance spectroscopy of the human forehead," Appl. Opt. vol. 46, pp. 1717-1725, April 2007.

[9] A. Ishimaru, *Wave Propagation and Scattering in Random Media.* Piscataway NJ: IEEE Press, ch.9, 1997.